JOURNAL OF MATERIALS SCIENCE 20 (1985) 989–995

The laser surface-alloying of iron with carbon

A. WALKER, H. M. FLOWER, D. R. F. WEST
Department of Metallurgy and Materials Science, Imperial College of Science and Technology, London SW7 2BP, UK

Observations are reported on the structure of iron, laser surface-alloyed with carbon. Repeated laser surface-melting of iron pre-coated with DAG graphite has produced layers containing up to ~ 6 wt % C, showing fine-scale white iron structures. Eutectic regions (interlamellar spacing ~ 0.5 μm) have been shown by transmission electron microscopy to consist of Fe_3C + ferrite, the latter having formed by decomposition of austenite during solid state cooling. Regions of fine pearlite (spacing ~ 55 nm) have also been observed. Carbon diffusion into the substrate during alloying produces a zone containing austenite and martensite.

1. Introduction

Laser surface-alloying is an area of growing technological interest aimed at enhancing properties such as wear resistance or corrosion resistance, the subject has recently been reviewed by Draper [1]. It offers a versatile approach to the production of surface layers of a wide range of structures and compositions on a variety of substrates. The structures can be of a fine-grained nature as a result of the relatively rapid cooling rates that can be achieved from the melt. A common technique is to pre-coat the substrate with the material to be alloyed and to control the laser melting parameters (power, beam diameter, traverse speed) to obtain the required depth of alloying. The literature of surface-alloying using ferrous substrates is not very extensive but various alloying elements, e.g. chromium, molybdenum and carbon have been used [2–4].

Carbon is of potential practical interest in producing high carbon surface layers of high hardness, and also in obtaining fundamental structural data on the high carbon rapidly solidified structures. In laser processing, graphite coatings have been used by some investigators to reduce the surface reflectivity and it has been found that substantial amounts of carbon can be introduced into steel substrates in this way [5, 6].

The research reported here forms part of an investigation using graphite coatings as a controlled means of obtaining alloy layers of various carbon levels and structures. Some results from this work have been reported elsewhere in which a range of white iron structures including hypoeutectic and hypereutectic compositions have been observed [6]. The present paper is concerned particularly with the microstructural and crystallographic features of the Fe–Fe_3C eutectic and of the heat-affected zones which adjoin the alloyed zones.

2. Experimental procedure

Surface-alloying was carried out using a 2 kW continuous wave (CW) CO_2 laser (Control Laser Ltd) typically operating at ~ 1.7 kW with argon gas shielding to prevent reaction with the atmosphere. Pure iron of analysed composition (wt %) C 0.016, Si < 0.02, Mn 0.12, S 0.007, P 0.06, Cr < 0.01, Mo < 0.005, Ni < 0.02 was used as a substrate. Plate samples ~ 15 mm thick were grit blasted to give a consistent surface finish, and were traversed relative to the laser beam at speeds from 10 to 50 mm sec^{-1} and with beam diameters from 1.5 to 4 mm, producing melt depths up to 2.5 mm.

Graphite coatings were applied either by painting the surface with DAG diluted with a binder, or with a slurry in which the DAG was less diluted: the thicker coatings produced by the slurry were covered with adhesive masking tape. Successive

0022–2461/85 $03.00 + .12

laser surface-melting using up to 12 runs was carried out on the same area, reapplying the DAG coating between each treatment.

Metallographic examination of sectioned specimens was carried out using light and electron microscopy (scanning and transmission). Etching for light and scanning electron microscopy used 2% nital or, for deep etching, a warm solution of higher concentration incorporating 1% hydrofluoric acid. Portions of the surface-alloyed zone were fractured and then deep etched for examination of the three-dimensional nature of the carbide phases. For transmission electron microscopy 3 mm discs were cut parallel to the top surface of the alloyed zone. After grinding they were ion-beam thinned for examination in a 1 MeV AEI EM7 electron microscope. The depths of the areas examined below the melt surface were not accurately determined: regions spanning the alloyed melt zones through to the parent metal heat-affected zone were included in the samples examined. X-ray diffraction examination of the surfaces of the laser-alloyed samples was carried out using a diffractometer.

3. Results

3.1. Light and scanning electron microscopy

Two uniformly mixed key hole laser melted zones, one hypoeutectic and the other hypereutectic, were examined.

The structures of these melt zones are illustrated in Figs. 1 and 2. In the hypoeutectic zone the austenite dendrites (Fig. 1) grow preferentially normal to the zone interface. Near the surface the primary arm spacing was $\sim 10\,\mu m$ and the secondary arm spacing $\sim 3\,\mu m$: the latter value is indicative of a cooling rate from the melt of $\sim 10^4$ K sec^{-1} [7]. The hypereutectic zone exhibits extensive porosity and cracking. Pro-eutectic cementite forms as faceted plates (Fig. 2) which grow edgewise, spreading through the melt zone. Each family of cementite plates originates from a common source at the melt interface and spreads in an apparently branched manner producing fan-shaped plate distributions.

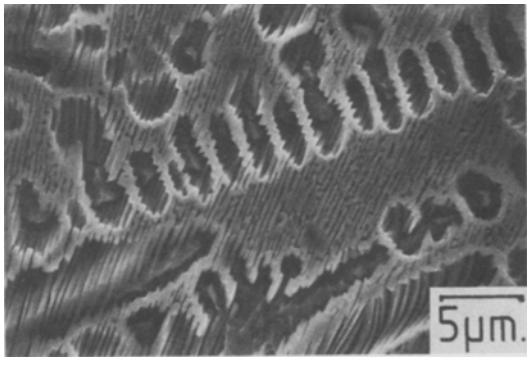

Figure 1 Hypoeutectic structure produced by laser surface-alloying of iron with carbon; austenite dendrites have been etched away showing the dendrite profile in the eutectic matrix.

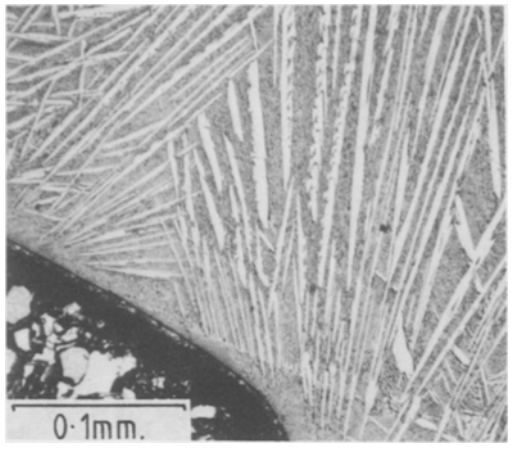

Figure 2 Hypereutectic structure produced by laser surface-alloying of iron with carbon; pro-eutectic Fe_3C plates (faceted) showing branching in the eutectic matrix.

The eutectic regions themselves show a lamellar (plate-type) morphology (Figs. 1 and 2) with apparent spacings in the range 0.3 to 0.8 μm: there is no clear size trend from one part of the melt zone to another. In the hypereutectic case each colony of the eutectic is oriented with the eutectic plates parallel to an adjacent primary cementite plate: this parallelism was confirmed using polarized light. Deep etching of fractured surfaces in the hypereutectic zone (Figs. 3a to c) shows clearly details of the growth modes. Fig. 3a shows the surface of a primary cementite plate which contains ridges and steps corresponding to positions of austenite growth from the plate surface. In Figs. 3b and c it can be seen that rods and ridges of cementite grow from the faces of the primary plates and by branching give rise to eutectic plates lying parallel to the parent cementite. Eutectic growth also occurs via growth from the edges of the primary plates as shown in Figs. 3b and c.

3.2. X-ray analysis

Fig. 4 shows the results from X-ray diffractometer

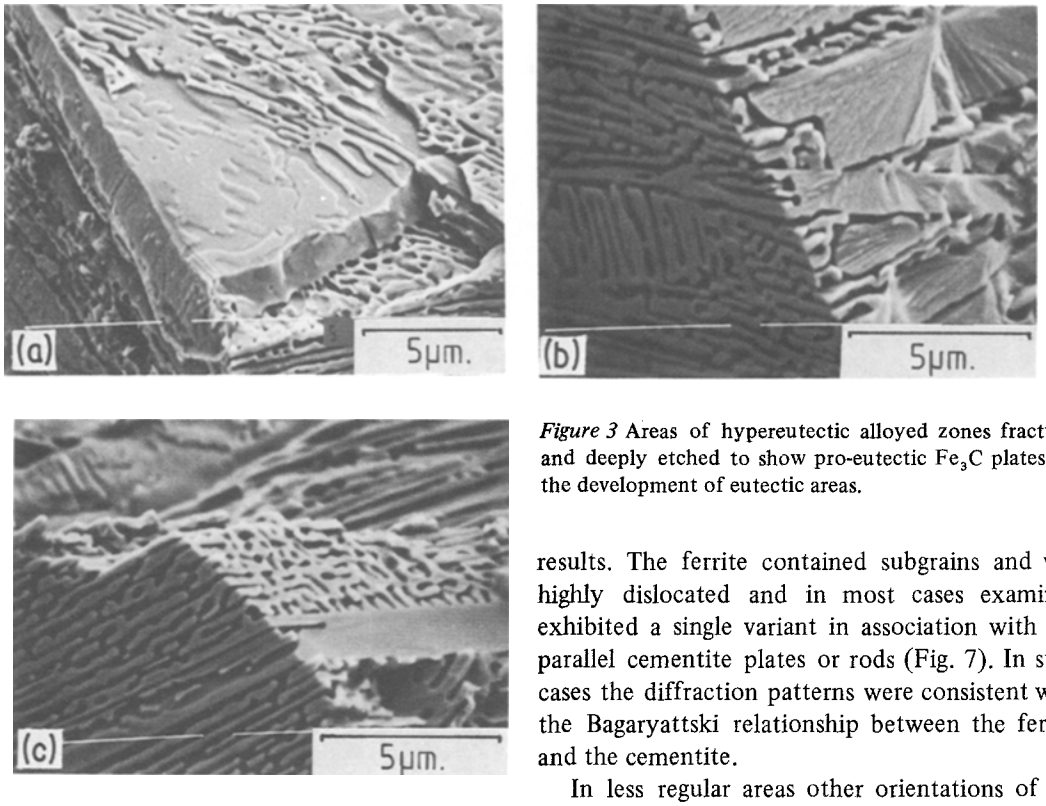

Figure 3 Areas of hypereutectic alloyed zones fractured and deeply etched to show pro-eutectic Fe_3C plates and the development of eutectic areas.

analysis of a region of hypereutectic composition produced by overlapping laser tracks. The reflections obtained from the as-laser-treated surface (Fig. 4a) were indexed in terms of ferrite and Fe_3C: however a few lines remained unaccounted for. Examination of the surface after grit-blasting showed only ferrite reflections (Fig. 4b). This is attributed to fracturing of the Fe_3C plates and smearing of the ferrite over the surface. Deep-etching removes the ferrite between the Fe_3C plates and diffractometry shows only Fe_3C reflections (Fig. 4c) and some unidentified lines.

3.3. Transmission electron microscopy

In the melt zone of both hypoeutectic and hypereutectic compositions the lamellar eutectic products were observed (Fig. 5) together with less regular regions containing rod-shaped carbide particles. In the most perfectly lamellar regions the width ratio of carbide–austenite phases was found to be $2 \pm 0.5:1$. Analysis of selected area diffraction patterns showed that the carbide is exclusively Fe_3C (Fig. 6), which in many cases contained stacking faults. The metallic phase was exclusively ferrite rather than retained austenite or martensite in the lamellar regions, thus confirming the X-ray results. The ferrite contained subgrains and was highly dislocated and in most cases examined exhibited a single variant in association with the parallel cementite plates or rods (Fig. 7). In such cases the diffraction patterns were consistent with the Bagaryattski relationship between the ferrite and the cementite.

In less regular areas other orientations of the two phases were observed which did not obey any simple relationship. Additionally in regions between well-ordered eutectic colonies the austentite was observed to have locally decomposed into pearlite of extremely fine (~ 55 nm) lamellar spacing (Fig. 8).

Examination of the heat-affected zone immediately adjacent to the melt zone showed evidence of carbon diffusion into the parent metal. (Fig. 9). The microstructure consisted of heavily dislocated retained austenite together with martensite plates (Fig. 10). Analysis of electron diffraction patterns showed that the martensite was related to the austenite by the Kurdjumov–Sachs relationship. The martensite diffraction patterns were clearly distorted from cubic symmetry. The errors of measurement of the electron diffraction patterns did not permit exact determination of the c/a ratio of the tetragonal martensite but measurements indicated at approximate value of about 1.04.

4. Discussion

The experimental results clearly show that even under the conditions of rapid solidification encountered in laser melting and alloying of the iron with carbon the high carbon content melt zone undergoes the equilibrium sequence of phase

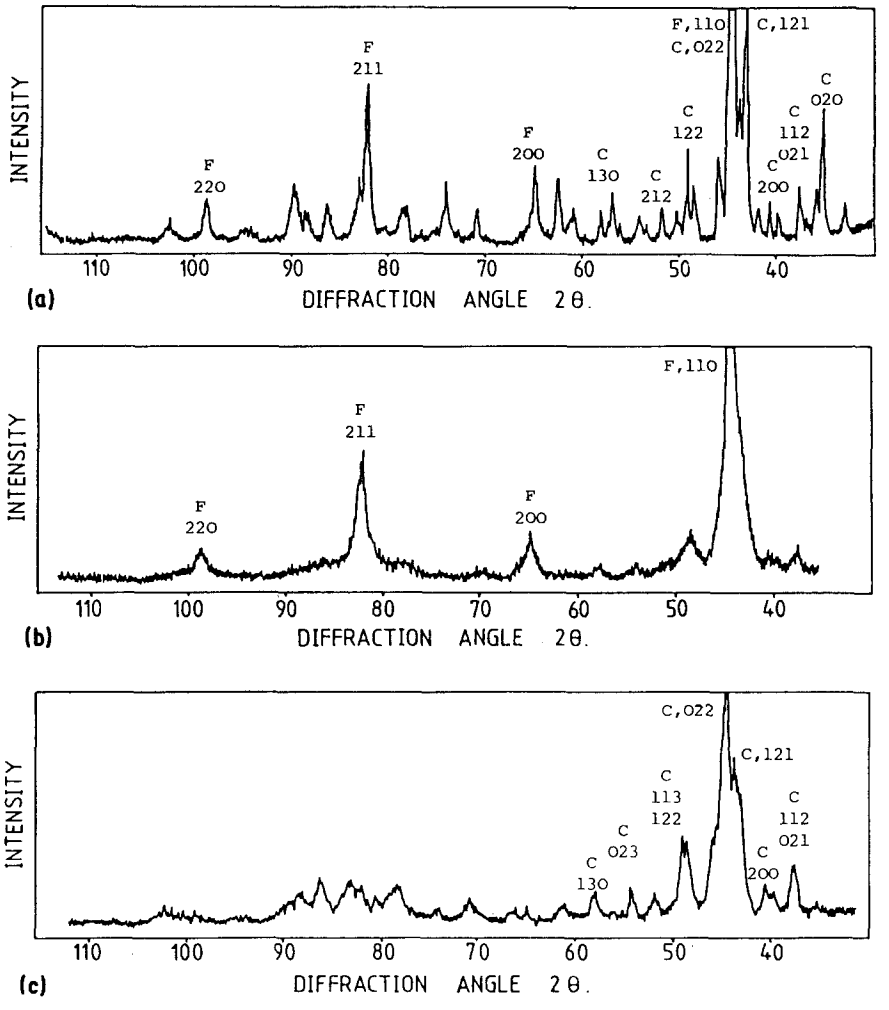

Figure 4 X-ray diffractometry data from surface of hypereutectic alloyed zone. (a) As-laser alloyed, (b) after grit-blasting the surface; (c) after deep-etching.

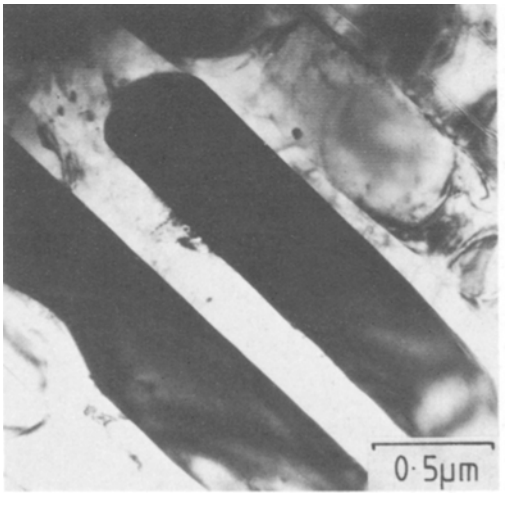

Figure 5 Transmission electron micrograph of the lamellar eutectic containing cementite and ferrite.

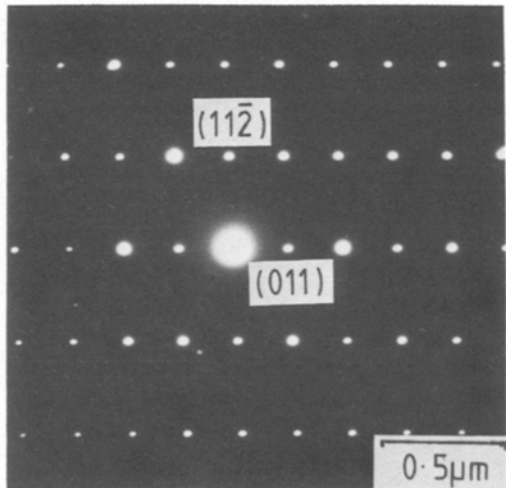

Figure 6 Selected area diffraction pattern of the orthorhombic Fe_3C in the eutectic.

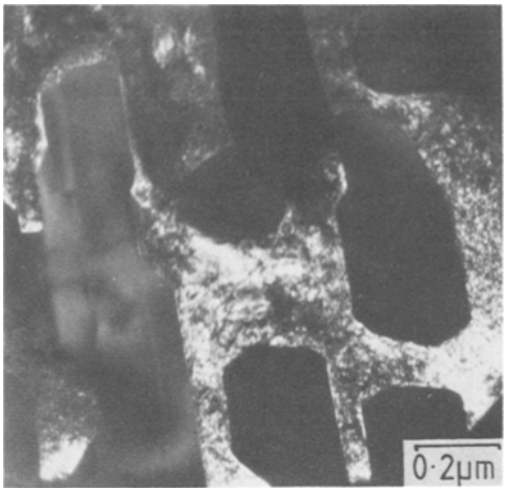

Figure 7 Dark-field electron micrograph of a eutectic region using a 1 1 0 ferrite reflection.

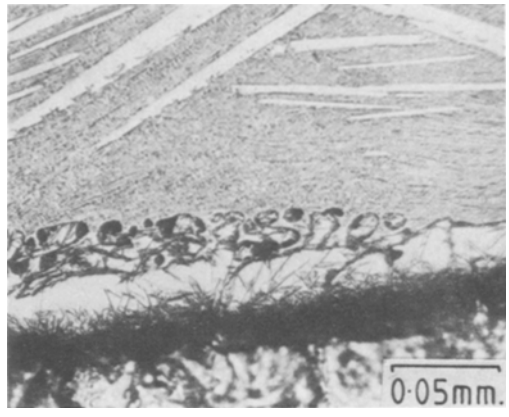

Figure 9 Region spanning the melt and heat-affected zones, the latter contains martensite and retained austenite.

transformations involving the austenite/cementite eutectic and subsequent diffusional decomposition of austenite to ferrite and cementite. Similar observations have recently been briefly reported for rapidly solidified cast irons produced by laser processing [6] and by melt spinning [8]. The transformations are considered in more detail below.

Hillert and Steinhauser [9] have carried out a detailed study of cast iron solidification using light microscopy on coarser structures than those produced by the laser melting in the present work. There are many points of similarity. The fan-like growth of primary cementite, attributed by Hillert to development from a common source via repeated nucleation on broken-off fragments of plates, is observed here as is the more uniform growth of austenite dendrites. The nucleation of the eutectic on primary cementite was also observed to involve the formation of two-dimensional dendrites of austenite on the broad faces of the plates as noted here (Fig. 3a). Rods and ridges of cementite also develop on these faces (Figs. 3b and c). The plate-like lamellar eutectic, which is the dominant growth morphology in the present work (cf. rods in Hillert's microstructures), develops by edgewise growth in a direction normal to the main growth direction of the rods and ridges. This involves repeated branching from them

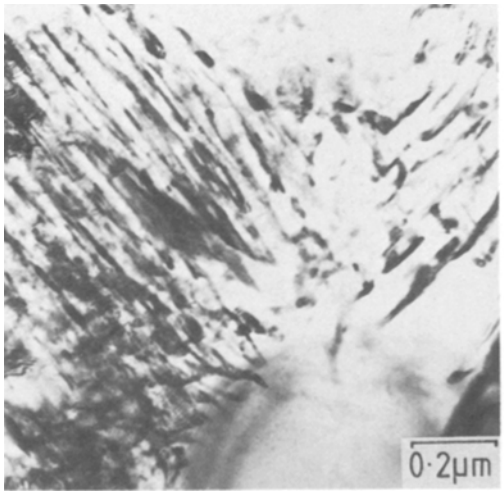

Figure 8 Fine pearlite formed by decomposition of austenite at the intersection of two eutectic colonies.

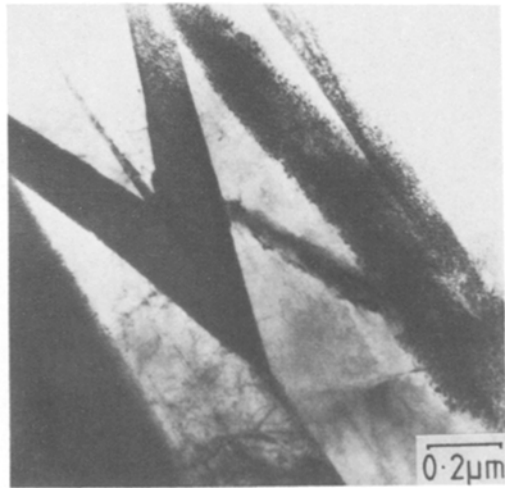

Figure 10 Martensite and retained austenite in the carbon-enriched parent metal heat-affected zone.

to produce plates crystallographically and morphologically parallel to the parent primary plate. This may be associated with the fact that the volume ratio of the γ and Fe_3C phases is close to 1, for which value lamellar growth has been shown to be favoured [10]. A second source of eutectic growth was also found in the present work: the edges of primary plates break up into eutectic lamellae during growth (Fig. 3c), again resulting in eutectic and primary plates being crystallographically and morphologically parallel. It is noteworthy that although plate growth may be expected to be most rapid in the direction of the steepest temperature gradient the crystallographic effects associated with the eutectic development can be dominant in determining the growth direction. There appear to be no such crystallographic effects associated with the nucleation of the eutectic in hypoeutectic material, although no detailed study has been made. It is presumed that it requires the nucleation of a layer of cementite around the primary austenite and that the effects of thermal gradients play a dominant role in determining the eutectic growth directions.

Simple application of the lever rule taking account of phase densities, indicates that at the eutectic temperature the ratio of austenite to cementite should be ~1:1 by volume. However, the observed ratio of plate widths at room temperature is closer to 1:2 and the austenite has been replaced by ferrite. Again using the lever rule a ratio of 1:2 by volume is expected for equilibrium ferrite and cementite derived from ledeburite and, given the similar densities of α and Fe_3C, this is in good agreement with observation. Clearly the austenite of the eutectic has decomposed diffusionally during cooling to room temperature by rejection of carbon to the existing Fe_3C plates which have thus thickened. Below the eutectoid temperature carbon rejection has continued. The observation that the ferrite typically exhibits a single orientation in association with a family of parallel Fe_3C plates and is related to the Fe_3C by the Bagaryattski relationship implies that the ferrite nucleates on the Fe_3C plate surfaces and grows into the remaining austenite. This might be expected to produce an increasing concentration of carbon in the austenite at the advancing α/γ interface (Fig. 11). However, since carbon diffusion in ferrite is very much faster than in austenite the concentration profile at the α/γ interface is probably controlled by the transport

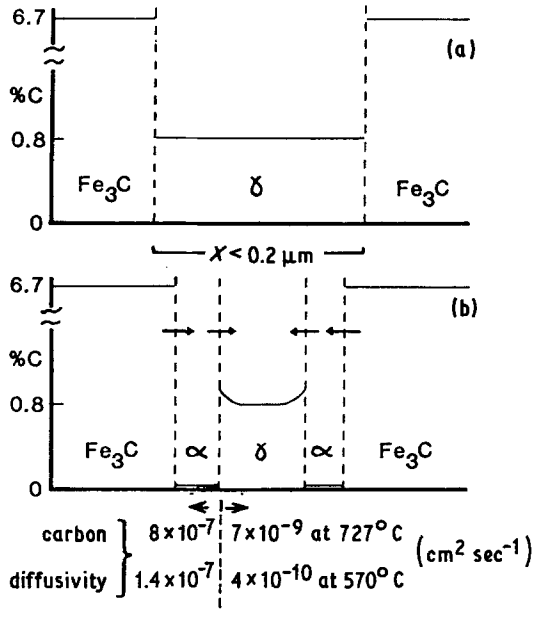

Figure 11 Eutectic structure and composition profiles at (a) 727° C and (b) between 727 and 570° C.

of carbon through the ferrite to the eutectic Fe_3C. The maximum diffusion distance involved is half the austenite plate width and must, therefore, be less than 0.2 μm.

This decomposition mechanism, although dominant, is not exclusively followed since small regions of extremely fine pearlite were also observed between well-ordered eutectic colonies. The cementite/ferrite plate width ratio was close to the ideal 1:7 for a eutectoid steel, again indicating that the austenite had equilibrated during cooling. The lamellar spacing of ~55 nm implies that the austenite was substantially undercooled when it transformed. Both Zener's [11] and Mehl's equations [12] predict a transformation temperature of about 570° C which lies close to the temperature of the nose of the TTT curve for a eutectoid steel. For such a transformation to occur the cooling rate must have been of the order of 100° C sec^{-1} (much higher and martensite or bainite could form, much lower and a coarser pearlite would be observed). Even at this rate carbon diffusion in ferrite is sufficiently fast to ensure complete transformation of austenite to ferrite in the lamellar eutectic regions by the mechanism shown in Fig. 11.

In addition to the dissolution of more than 4% carbon into the melt zone the microscopical study clearly demonstrates carbon diffusion in the solid

state into the unmelted parent low carbon steel. In the light micrographs retained austenite can be seen on the edge of the heat-affected zone immediately adjacent to the melt zone and within the austenite an increasing volume fraction of martensite is observed towards the parent metal (Fig. 10). The total width of this zone is 20 to 30 μm. Transmission electron microscopy confirmed the presence of retained austenite in this zone, indicating a carbon content in excess of 0.7 wt%. The Kurdjumov–Sachs orientation relationship observed between the martensite and the austenite implies that the carbon content is below 1.4 wt%, since at higher carbon levels the orientation relationship is changed [13]. The very approximate *c/a* ratio measured for the martensite is consistent with these observations and indicates a carbon content of about 1 wt%. This carbon must have diffused into the parent metal from the fusion zone during solidification and subsequent cooling to room temperature. The problem of calculating carbon diffusion into iron at the melt zone liquid–solid interface is not feasible in view of the large number of variable parameters involved but it is of interest to note that a layer 20 to 30 μm deep can be produced containing ~ 1% carbon during the laser treatment.

5. Summary and conclusions

Rapidly solidified white iron structures of both hypoeutectic and hypereutectic compositions have been produced by the laser surface-melting of pure iron pre-coated with DAG graphite. The eutectic regions show both plate-like and rod-like morphologies, and in the hypereutectic composition range the eutectic nucleates and grows by a branching process from pro-eutectic Fe_3C; the interlamellar spacing is typically ~ 0.5 μm. The eutectic solidifies as austenite + Fe_3C, but on cooling in the solid state austenite transforms to ferrite to produce a lamellar ferrite + Fe_3C structure: some areas of austenite transform to a pearlite of very fine spacing (~ 0.55 nm). During laser processing carbon diffusion into the substrate occurs producing an austenitic + martensitic region.

Acknowledgements

Acknowledgements are made to the SERC and to Rolls Royce Ltd, Barnoldswick for support, including the award of a research studentship to one of the authors (AW). The authors are also grateful to Dr W. M. Steen for his participation in the work and to the National Physical Laboratory and the British Steel Corporation for supplying pure iron.

References

1. G. W. DRAPER, *J. metals* 6 (1982) 24.
2. D. S. GNANAMUTHU, in "Applications of Lasers in Materials Processing II", edited by E. A. Metzbower (American Society for Metals, Metals Park, Ohio, 1979) p. 177.
3. G. CHRISTODOULOU and W. M. STEEN, in "Lasers in Materials Processing" edited by E. A. Metzbower (American Society for Metals, Metals Park, Ohio, 1983) p. 116.
4. T. R. TUCKER, A. H. CLAUER, S. L. REARN and C. T. WALTERS, in "Rapidly Solidified Amorphous and Crystalline Alloys", edited by B. H. Kear, B. S. Giessen and M. Cohen (Elsevier Science Publ. Co., Amsterdam, 1982) p. 541.
5. M. CARBUCICCHIO, G. MEAZZA, G. PALOMBARINI and G. SAMBOGNA, *J. Mater. Sci.* 18 (1983) 1543.
6. A. M. WALKER, D. R. F. WEST and W. M. STEEN, *Met. Technol.* 11 (1984) 399.
7. M. IBARAKI, J. OKAMOTO and H. MATSUMOTO, *J. Jpn Inst. Metals* 32 (1968) 396.
8. S. B. NEWCOMB, R. A. RICKS, D. R. BURY and R. W. K. HONEYCOMBE, in "Electron Microscopy and Analysis 1983", Institute of Physics Conference Series 68 (Institute of Physics, Bristol, 1984) p. 315.
9. M. HILLERT and H. STEINHAUSER, *Jernkont. Ann.* 144 (1960) 520.
10. D. J. S. COOKSEY, D. MUNSON, M. P. WILKINSON and A. HELLAWELL, *Phil. Mag.* 10 (1964) 745.
11. C. ZENER, *Trans. AIME* 167 (1946) 550.
12. G. E. PELISSIER, M. F. HAWKES, W. A. JOHNSON and R. F. MEHL, *Trans. ASM* 30 (1942) 1049.
13. R. W. K. HONEYCOMBE, "Steels: Microstructure and Properties" (Edward Arnold, London, 1981).

Received 27 March
and accepted 12 May 1984